Weak acids with super-electron-donor dimetal complexes: Synergy in bifunctional activity

Matthew E. Humphries, Emily S. Wusterbarth, Dennis L. Lichtenberger*

Department of Chemistry and Biochemistry, The University of Arizona, Tucson, Arizona, 85721, USA

We dedicate this work to Professor William D. Jones on the occasion of his 65th birthday.

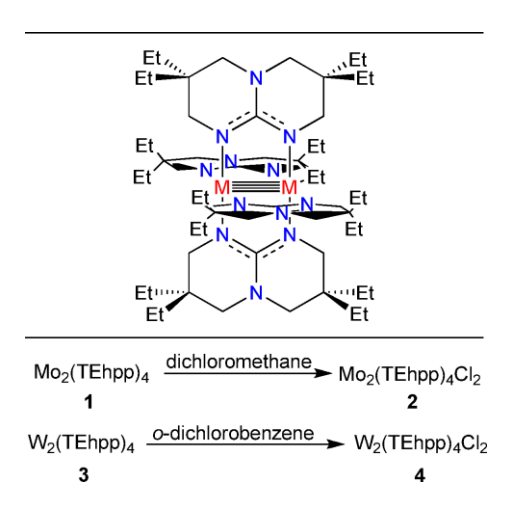
ABSTRACT: Dimetal paddlewheel complexes with bicyclic guanidine ligands are extremely strong thermodynamic electron donors. As a probe of the chemical potential and sites for chemical reactivity of these complexes, the interaction of $Mo_2(TEhpp)_4$ with weak acids was investigated (TEhpp is the anion of the bicyclic guanidine 3,3,9,9-tetraethyl-1,5,7-triazabicyclo[4.4.o.]dec-4-ene). $Mo_2(TEhpp)_4$ is readily protonated by acetic acid and trifluoroacetic acid as expected, but surprisingly by a mechanism that is more complicated than a simple acid-base proton exchange. Electrochemistry measurements of the shifts in potentials with successive additions of acid reveals that the conjugate base of the acid plays a critical role throughout the reaction. Computations indicate that initially the acid hydrogen bonds to a TEhpp nitrogen atom bound to the metal, and then a facile rearrangement of the conjugate base toward the axial site of the Mo–Mo bond concomitantly results in protonation of the nitrogen atom. Interestingly, the dimetal complex is bifunctional in this process, acting as a nucleophile at the nitrogen atoms of the TEhpp ligands, and as an electrophile at the Mo–Mo axial bond sites. The protonation requires a novel synergism of these disparate bonding interactions, in which protonation is not favored without enhancement by the coordinated base, and coordination of the base is enhanced by the protonation.

Keywords: dimetal, quadruple bond, electrochemistry, reductant, protonation:

1. Introduction

The complexes $Mo_2(TEhpp)_4$ 1 and $W_2(TEhpp)_4$ 3 have extremely low gas-phase vertical ionizations energies for neutral molecules of 4.31 eV for 1 and 3.71 eV for 3, the latter being lower than cesium.[1,2] These low electron detachment energies are unique to the bridging bicyclic guanidinates because of their destabilizing interaction with the δ -orbital of the M_2^{4+} core.[3] In the oxidized M_2^{5+} core, the guanidinates act as a source of stabilization via π -donation into the δ -orbital hole. These low electron detachment energies translate to extremely negative (low energy) solution oxidation potentials[2,4] for 1 (-1.83 V) and 3 -2.34 V) relative to the oxidation potential of ferrocene (the reference for all potentials reported in this paper). These potentials are on either side of the commercially available $Co(Cp^*)_2$ (-1.94 V in dichloromethane[5]), which is a common strong chemical reductant in organic solvents. Neutral organic molecules that are termed super-electron-donors generally have oxidation potentials more negative than about -0.8 V.[6]

These complexes are expected to have a rich chemistry, and there are hints of this chemistry from indirect observations in the literature. Dissolution of 1 and 3 in dichloromethane and o-dichlorobenzene, respectively, yields $Mo_2(TEhpp)_4Cl_2[4,7]$ and $W_2(TEhpp)_4Cl_2[2]$ (Scheme 1). In each case a difficult dechlorination of either alkyl or aryl chlorides takes place. Another example shows H_2 production takes place through the reduction of Hhpp in the course of the synthesis of $W_2(hpp)_4$ (hpp is the non-alkylated, less soluble analogue to TEhpp).[8] Surprisingly, further chemical reactivities of these materials have yet to be explicitly explored. These preliminary observations demonstrate the potential for difficult processes like dehalogenation and cross-coupling reactions, or more simple processes like the hydrogen evolving reaction (HER).



Scheme 1. The reactivity of 1 and 3 towards dechlorination of C–Cl bonds of dichloromethane and o-dichlorobenzene, respectively.

The aim of the current study is to characterize the sites, mechanisms, and energies of interaction of protons with $Mo_2(TEhpp)_4$ as an initial step in an extended investigation of the reduction of protons from weak acids to molecular hydrogen by dimetal paddlewheel complexes. Of course, the hydrogen evolving reaction (HER) is receiving intense study from numerous directions.[9] An advantage of the dimetal paddlewheel complexes for this study is that they have a relatively rigid, well-defined structure to serve as a template on which the chemistry takes place, with little change in structure as a function of the active oxidation states that involve addition and removal of electrons from the dimetal δ -bond orbital. These systems also show the ability to tune the chemical potential with only moderate change in structure. $Mo_2(TEhpp)_4$ 1 allows characterization of the interaction of the dimetal complex with low concentrations of acetic acid without catalytic production of hydrogen. The electrochemical results reported in this study were not anticipated and required detailed computational evaluation. Future studies of $W_2(TEhpp)_4$ 3, which has the potential to produce hydrogen electrocatalytically, build on the new insights gained from compound 1.

In addition, a significant update to the cyclization of the triamine 5 to form HTEhpp 6 with improved yields is included in this study. This new synthetic route provides a more accessible and reproducible approach towards synthesizing bicyclic guanidines.

2. Materials and methods

2.1 General procedures

Mo₂(TEhpp)₄ 1 was synthesized according to the literature.[4] All procedures were carried out using rigorous Schlenk techniques with argon unless otherwise noted. The triamine, N, N-bis(3-amino-2,2-diethyl-propyl)amine, was synthesized according to the literature.[10] Guanidine hydrochloride was recrystallized in methanol and dried *in vacuo* prior to use. Trifluoroacetic acid was purchased from Fisher Scientific. For electrochemical studies, the trifluoroacetic acid was distilled over P_2O_5 and degassed using the freeze-pump-thaw method. The concentration of n-BuLi was determined via titration with diphenylacetic acid prior to use. Toluene was purchased extra dry over molecular sieves and degassed using the freeze-pump-thaw method. THF (unstabilized) was purchased from Fisher Scientific, distilled over Na/benzophenone, dried over 3 Å sieves, and degassed using the freeze-pump-thaw method. All solvents were stored in a Strauss flask fitted with a Kontes valve. Acetic acid (99.998 %) was purchased from Fisher Scientific, transferred to a 5 mL Schlenk tube and freeze-pump-thawed.

2.2 Synthesis of 3,3,9,9-tetraethyl-1,5,7-triazabicyclo[4.4.0]- dec-4-ene (HTEhpp)

The cyclization of the triamine uses a similar procedure described in the literature. [11] To a 10 mL round bottom flask was added *N,N*-bis(3-amino-2,2-diethyl-propyl)amine (0.9723 g, 4 mmol) along with guanidine hydrochloride (0.4197 g, 4.4 mmol). The flask was fitted with a condenser, and the mixture was pump-purged. After stirring for 15 min, trifluoroacetic acid (0.15 mL, 2 mmol) was added. After which, all solids dissolved and the solution was stirred at 175 °C overnight. The next day the solution was cooled to 70 °C open to air and 4 mL methanol was added followed by 1.7 eq NaOMe with stirring. The cloudy mixture was concentrated *in vacuo*, 10 mL dichloromethane was

added and the mixture was filtered. Concentration of the filtrate and washing with hexanes yielded the ligand HTEhpp (1.4 mmol, 36%). This compound can be recrystallized with toluene.

2.3 Electrochemical materials and methods

Electrochemical data were collected using Gamry Interface 1000 and Gamry Reference 3000 potentiostats with the Gamry Framework 6 software. All electrochemical studies were conducted either under a positive Ar atmosphere or inside a glovebox using a custom 4-necked flask. A 3-electrode setup was employed with a silver wire reference electrode separated from the bulk solution by a Vicor glass frit, a 3 mm diameter disc glassy carbon working electrode, and a Pt counter electrode. Ferrocene was used as an internal reference throughout the experiments. All solutions were 0.3 M n-Bu₄NPF₆ in THF (10 mL) and prepared in the glovebox. Acetic acid was dispensed via 10 μ L or 200 μ L Eppendorf auto pipettes. Successive CV scans were reproducible without electrode polishing between scans.

2.4 Computational Methods

DFT computations were performed using the Amsterdam Density Functional (ADF) software version 2017.107.[12–14] The basis set was valence Slater-type function triple-zeta (inner shells treated as core) with one polarization function for all atoms (TZP) adapted for relativistic corrections according to the zeroth-order relativistic approximation (ZORA),[15,16] as available in the ADF package. The geometries and energies of $Mo_2(hpp)4$ were initially refined in THF solution (the solvent for experiments) with the PBE functional[17] with dispersion corrections according to the method of Grimme using the BJ damping function (PBE-D3-BJ).[18] Solvation Gibbs energies are estimated by the conductor-like screening model (COSMO) of solvation[19,20] using the Delley surface[21] with atomic van der Waals radii from Allinger,[22] the default dielectric constant of 7.58 for THF, and r_{solv} for hydrogen for determining the solvent accessible surface[23] set to 1.2 Angstroms[24].

The Mo₂(TEhpp)4 complex was modeled by Mo₂(hpp)4, in which the ethyl groups were replaced by hydrogen atoms in order to significantly reduce the computational time. Geometry optimization of the dimolybdenum complex started from the crystal structure of Mo₂(hpp)4[25] adjusted to C₄ symmetry. The structure is close to D₄ symmetry but the slightly nonplanar central N atoms of the hpp ligands reduces the symmetry to C₄. The experimental (and calculated in THF) Mo-Mo bond distance is 2.07 (2.13) Å and the average Mo-N bond distance is 2.16 (2.15) Å. Subsequent computations found that the energies in this model were matched within 0.1 eV with much less computational time by gas phase geometry optimizations followed by single point solvation energies, and by gas phase frequency computations at the lower level of the VWN functional and double-zeta functions on all but Mo. The latter model was used for all energies reported in this work.

Calculations of the Gibbs energies, oxidation potentials, and equilibrium constants for reactions included the optimized electronic energies calculated by the PBE-D3-BJ/TZP method described above, the zero-point vibrational energies unscaled from harmonic frequency calculations at the lower VWN level, and the corresponding thermal enthalpy and entropy contributions in solution at 298.15 K. Uncorrected gas phase translational and rotational entropies can introduce substantial error in the determination of Gibbs energies for solution reactions, especially in cases where the number of reactant molecules and product molecules differ.[26] The solution translational and rotational entropies were estimated as described and tested before, in which the gas phase values are scaled by one half, and associative and dissociative reactions include explicit solvent interactions to cancel entropy errors from reactants to products.[26]

Figures of the optimized geometries, molecular orbitals, and the charge potential surface were created with the program Visual Molecular Dynamics.[27]

3. Results and Discussion

3.1 Synthesis

Inconsistent results in cyclizing *N*,*N*-bis(3-amino-2,2-diethyl-propyl)amine **5** to form HTEhpp **6** using CS₂ as a carbon source led us to explore other sources, namely guanidine hydrochloride **8** (Scheme 2). Previous synthesis of **6** required CS₂ and *p*-toluenesulfonic acid in *p*-xylene solvent.[10] Moving to **8** allowed for a simpler procedure where no solvent was necessary. Use of trifluoroacetic acid as an acid catalyst instead of *p*-toluenesulfonic acid proved much simpler to remove. If necessary, toluene can be used as a recrystallization solvent. Complex **1** was synthesized according to the literature via a rapid substitution reaction in which the guanidinate displaces the

acetates from Mo_2 (trifluoroacetate)₄ at room temperature in THF and precipitates at -30 °C. The precipitate can be washed with cold toluene to obtain pure 1.

Scheme 2. Cyclization of **5** to form the ligand HTEhpp **6**.

3.2 Electrochemical characterization of 1

The first two oxidation potentials of 1 were previously measured using differential pulse voltammetry (DPV)[4], which showed two chemically reversible redox processes at -1.83 and -1.05 V vs Fc/Fc⁺ for Mo₂^{4+/5+} and Mo₂^{5+/6+}, respectively. The cyclic voltammogram of 1 presented in Fig. 1 provides additional information. Note that the scans begin at very negative potentials of around -2 V relative to the oxidation of ferrocene (Fc/Fc⁺) and sweep positive. The need to start at this very negative potential underscores the ease of oxidation and by corollary the strong reducing power of this complex. There are two chemically reversible redox processes for 1. The first redox couple, Mo₂^{4+/5+}, occurs at E_{1/2} = -1.77 V vs Fc/Fc⁺ and the second, Mo₂^{5+/6+}, at E_{1/2} = -1.00 V. The intensities of the peaks showed a linear dependence on the square root of the scan rate consistent with a diffusion-controlled homogeneous solution process (see Supporting Information, SI). An overlay of multiple sequential scans showed less than 1% change in current, so the surface of the electrode was not being altered and polishing of the electrode between scans was not necessary. The two electrons in these redox processes originate from the M–M δ –bond orbital, and thus as the complex becomes oxidized from Mo₂⁴⁺ to Mo₂⁶⁺ the quadruple bond weakens to a triple bond.

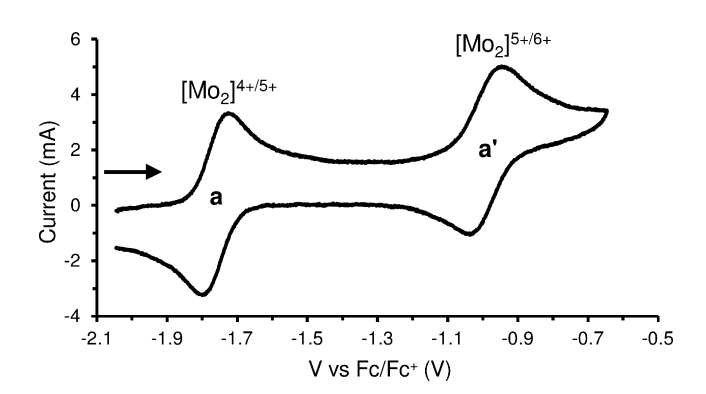


Fig. 1. Cyclic voltammogram of 1.1 mM 1 in 0.3 M nBu₄NPF₆ THF with $E_{1/2}$ values of -1.77 V for $[Mo_2]^{4+/5+}$ and -1.00 V for $[Mo_2]^{5+/6+}$ on a glassy carbon electrode (A = 0.071 cm²) at 100 mV s⁻¹ scan rate.

3.3 Electrochemical studies of 1 with acetic acid

Acid studies were conducted via cyclic voltammetry by incremental additions of low acid concentrations (i.e. 1-4 equivalents) of acetic acid. These additions provided evidence of the formation of several species in equilibrium in solution (Fig. 2). The measured oxidation potentials are collected in Table 1. The bottom of Fig. 2 contains the CV of

1 from Fig. 1 without acid. Addition of 1 equivalent of acetic acid produces a new quasi-reversible oxidation peak **b** (red trace). The peaks a and a' representing the $[Mo_2]^{4+/5+}$ and $[Mo_2]^{5+/6+}$ redox couples from 1 persist, suggesting an equilibrium between 1 and a species resulting from the interaction of acetic acid with 1. The concentration and kinetics of the equilibrium process allow observation of both the original and interacted species. The nature of this interaction is clarified in the following section. When the acid concentration is doubled to 2 equivalents the current of peak **b** increases (blue trace), as expected for a shift of equilibrium toward the species with acid interaction with 1. Additionally, a new chemically reversible peak c appears corresponding to a third species in solution. The shift in oxidation potential from **b** to **c** is similar to the shift from **a** to **b**, suggesting **c** represents the oxidation of a new species resulting from a second acetic acid interaction with the complex. The hint of additional oxidation current in the vicinity of -0.7 to -0.8 V that appeared with the addition of one equivalent of acid now becomes a clear quasireversible oxidation peak \mathbf{d} with the addition of two equivalents of acid. The shift of peak \mathbf{d} from peak \mathbf{a} is similar to the shift of peak **b** from peak **a**, suggesting that peak **d** corresponds to the second oxidation of the species resulting from acetic acid interaction with the complex. The original redox events from 1 are no longer present once 4 equivalents of acetic acid are added (grey trace). Peak **b** remains, peak **c** increases, and peak **d** is now the highest current in the CV, indicating substantial shifts in the equilibrium concentrations toward species with acetic acid interacting with 1. Although peak \mathbf{d} is now electrochemically irreversible with excess acid concentration, perhaps due to excess protonation of an hpp ligand and partial or complete dissociation, the species that oxidized in regions c and b are observed on the return reduction through these potentials, indicating that the overall process starting from -2 V and back is chemically reversible.

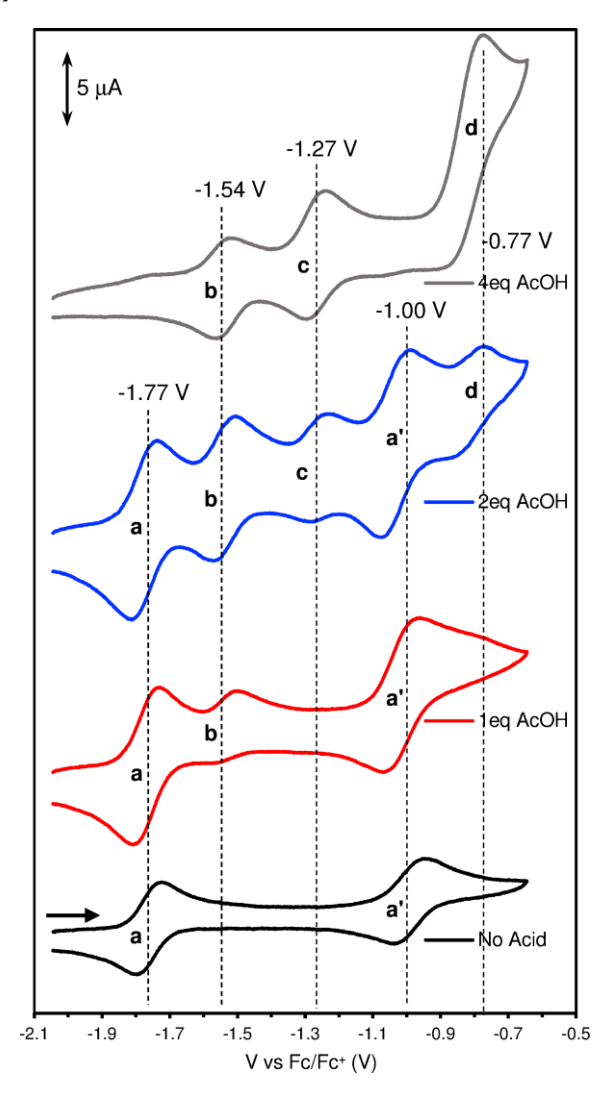


Fig. 2. Cyclic voltammograms of 1 interacting with increasing concentrations of acetic acid. Black trace shows both redox events of 1 with no acid. The following traces show new quasi-reversible peaks indicating association of the acid to 1: red trace, 1 eq. acid; blue trace, 2 eq. acid; grey trace, 4 eq. acid. (See Fig. 1 for conditions)

Table 1. Experimental redox potentials of 1, 1 in the presence of acetic acid (AcOH), and 1 in the presence of trifluoroacetic acid (TFA).

	Peak Label	E _{1/2} (V vs Fc/Fc ⁺)
$[Mo_2]^{4+/5+}$	a	-1.77
$[Mo_2]^{5+/6+}$	a'	-1.00
$[AcOH][Mo_2]^{4+/5+}$	b	-1.54
$[AcOH]_2[Mo_2]^{4+/5+}$	c	-1.27
$[AcOH]_{1,2}[Mo_2]^{5+/6+}$	d	-0.82
$[TFA][Mo_2]^{4+/5+}$	e	-1.38
$[TFA][Mo_2]^{5+/6+}$	f	~-0.65

3.4 Interaction of acetic acid with 1

Several different interactions of acetic acid with 1 were explored computationally. Coordination of neutral donor Lewis bases to the axial sites of M_2^{4+} cores, namely THF, has been shown.[2,28] Anionic donors (Cl, TFPB) also occur, but only in the complexes with ligand systems that support M_2^{6+} cores such as 1 and 3.[2,7,26] Consequently, acetate coordination through its oxygen atom to the axial sites was considered, but computations indicate that acetate substitution for THF at the axial sites is not favored:

$$Mo_2(hpp)_4(THF)_2 + AcOH \rightleftharpoons$$

$$Mo_2(hpp)_4(THF)(AcOH) + THF \quad \Delta G = 8 \text{ kcal/mol}$$

The Gibbs energies of all species in the above reaction are determined with their solvation Gibbs energies in THF solution as described in the experimental section. An important factor in this consideration is the solvation energy of acetic acid in THF. In addition to the polarization and other contributions to the solvation energy in the continuum model for solvation, acetic acid has an explicit hydrogen bonding interaction between its OH group and the oxygen atom of THF:

$$AcOH \cdot \cdot \cdot OC_4H_8 \rightleftharpoons AcOH + OC_4H_8 \qquad \Delta G = \sim 7 \text{ kcal/mol}$$

The solvent hydrogen bond acceptor (HBA) ability of THF is even greater than that of water (0.48 vs. 0.35).[31] As a consequence of these implicit and explicit (H-bonding) solvation energies, dimerization of acetic acid is very small at these concentrations (0.1% by these computations). The energy to break this hydrogen bond is included in the equilibrium of the association of acetic acid with 1 in the equation above and in all subsequent equilibria involving solvated acetic acid discussed below.

Even if association of the oxygen atom of acetic acid to the axial site of the metal-metal bond were favored, the addition of this Lewis base would not explain the increasing difficulty of oxidation with addition of acid. The more positive oxidation potential with acid addition indicates a stabilization of the electron density in the complex.

Protonation of 1 is a natural expectation that would stabilize the charge density, and was considered as shown by the calculated Gibbs energies in Table 2. Structures of all species can be viewed in the Supporting Information and the Cartesian coordinates are provided for viewing in modeling programs. Of the five sites investigated, the most favored protonation site was at the N_b atoms of the TEhpp ligand (i.e. N bound to M0). This follows from the N_b atom being the most negatively charged atom in the complex (charge control for protonation) and also having direct overlap with the δ -orbital to give it some character in the HOMO (frontier orbital control). Surprisingly however, as Table 2 shows, none of the protonation sites are favored for direct proton abstraction from acetic acid.

Hydrogen bonding of the OH group of AcOH with the nitrogen atoms of the hpp ligands is weakly favored (Table 2) and some stabilization of the charge density leading to more positive oxidation potentials of the complex are found, but the hydrogen bonds are not sufficiently strong to account for the equilibria observed in the CVs. In particular, for the addition of two equivalents of acetic acid, the CV experiment shows an oxidation for the interaction of a second acid with the complex, but the computations do not predict the addition of a second

hydrogen-bonded acetic acid to the complex. The addition of a second hydrogen-bonded acetic acid to the complex is calculated to be disfavored by 7 kcal/mol relative to acetic acid in solution.

Table 2. Computed Gibbs energies (kcal/mol) of one equivalent of acetic acid (AcOH) interacting with Mo₂(hpp)₄ in THF at 298°K.

Protonation: $Mo_2(hpp)_4 + AcOH \rightleftharpoons [HMo_2(hpp)_4]^+ + AcO^-$		
Hydrogen location in product	kcal/mol	
M-H axial	26	
μ -H $-M_2$	24	
M-H (delta lobe)	15	
N_c – H	13	
N_b – H	1	
Association: $Mo_2(hpp)_4 + AcOH \rightleftharpoons$ $"Mo_2(hpp)_4(H)(OAc)"$		
Associated structure	kcal/mol	
AcOH H-bonded to M2 axial site	6	
AcOH H-bonded to N _c	-2	
AcOH H-bonded to N _b	-4	
N_b -H bond formed, acetate axial	-7	
See figures for optimized structures. N _b is a		

See figures for optimized structures. N_b is a nitrogen atom of hpp bound to Mo, N_c is a central nitrogen atom of hpp. Each energy includes the energy to break the H-bond of AcOH with THF in solution, $\Delta G = 7$ kcal/mol, and the protonations include product stabilization by H-bonding to THF.

The optimum interaction of acetic acid with 1 is found to be a combination of protonation of the N_b atom (N bonded to the metal) and association of the acetate ion with one oxygen of the acetate at the M–M axial site and the other oxygen atom directed toward the hydrogen atom of the H–N_b group (see Fig. 3). This structure reveals a synergistic interaction for this type of paddlewheel complex, which draws some similarities with the intramolecular deprotonation in the concerted metalation-deprotonation mechanism (CMD).[32,33] The interaction for the protonation of 1 is more closely associated with the proposed carboxylate exchange mechanism, which involves acid attack of the bound carboxylate leading to labilization and replacement of the bound carboxylate with the excess carboxylate:[34,35]

 $Mo_2(O_2CMe)_4$ + excess $HO_2CR \rightarrow Mo_2(O_2CR)_4$ + displaced HO_2CMe

In contrast to the carboxylates, the guanidinates in this work are far more basic and bind tighter to the dimetal core. Here the association of the acetate ion with the axial site helps promote protonation, and in turn the protonation helps promote acetate ion association with the axial site. The protonation does not occur without association of the acetate ion. The concept also bears a relationship to a frustrated Lewis pair (FLP),[36] where the Lewis base site of the guanidinate is separated from the Lewis acid axial site of metal-metal bond by the constraint of the geometry, and the two act together to allow protonation. The protonated structure with associated acetate can be written as $Mo_2(hpp)_3(Hhpp)(OAc)$, but it should be remembered that the acetate association in this formula is essential for stabilization of the protonated N_b atom.

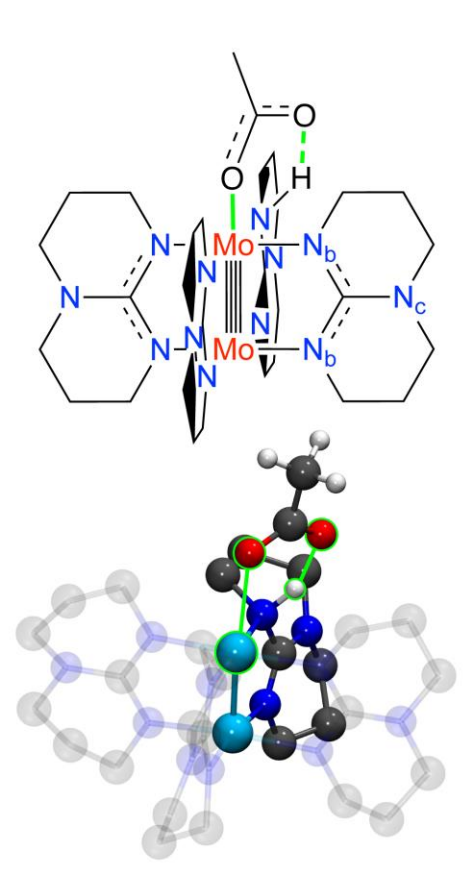


Fig. 3. Simplified bond line structure (top) and converged geometry (bottom) of the synergistic interaction where protonation at the nucleophilic position N_b on the bicyclic guanidinate is interdependently promoted by acetate bonding to the electrophilic Mo–Mo axial site with one oxygen, and the N_b –H group is H–bonding with the other oxygen atom of the acetate. The green lines show the interactions, and the other hydrogen atoms of the hpp ligands are omitted for clarity.

Mechanistically the initial attraction of the acetic acid to the complex is the hydrogen bonding of the OH group with the negatively charged N_b atom of the complex. After the acetic acid transitions from a solvated species with hydrogen bonding to THF to association with the metal complex, there are several paths differing by only a few kcal/mol that lead to the protonated complex depicted in Fig. 3. Two lowest-energy paths are shown in Fig. 4. Path a is an approach toward the vacant axial site of the metal-metal bond with the acetic acid favoring an orientation with the oxygen atom directed toward the vacant site and the O-H bond vector pointing toward an N_b atom of an hpp ligand. This axial approach leads to concerted protonation of the N_b atom and coordination of the acetate at the axial position (structure in Fig. 3). At long distances the initially favored approach is path $\bf b$ which is side-on to the complex with the O-H bond vector of the acetic acid perpendicular to the Mo-Mo bond vector and pointed at the N_b atom (images of these geometries are shown in the SI and coordinates are provided that animate the full path). In this perpendicular approach the oxygen atom is far from the axial site, but when the N_b -H distance shortens to ~1.2-1.4 Å the oxygen atom can bend to the axial site with only less than 2 kcal/mol activation energy above path $\bf b$. Fig. 4 shows that the protonated species is rapidly stabilized only when the approach of the H atom of the acetate to the N_b atom and the approach of the O atom of the acetate to the axial site are acting together synergistically (solid purple line).

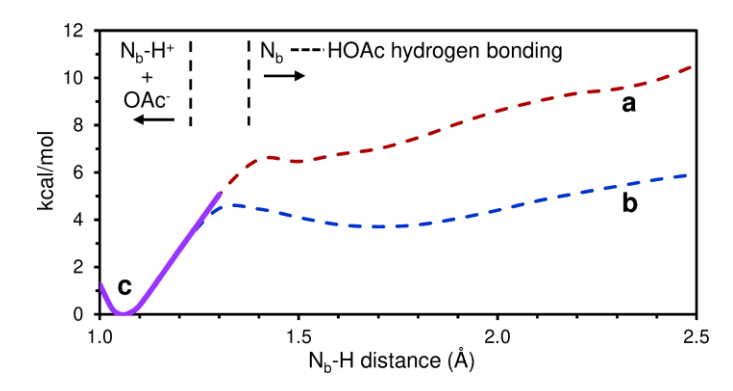


Fig. 4. Energy profile for association facetic acid with $Mo_2(hpp)_4$. Path **a** is an approach of acetic acid toward the vacant axial site of the metal-metal bond. Path **b** is an approach of acetic acid perpendicular to the metal-metal bond and pointed at H-bond formation with an N_b atom of hpp. Region **c** is the synergistic stabilization obtained with acetate simultaneously oxygen-coordinating at the axial site and protonating the N_b site.

The protonated $Mo_2(hpp)_3(Hhpp)(OAc)$ structure (Fig. 3) leads to a straightforward account of the trends in the CVs as a function of acid concentration as shown in Scheme 3. The left column shows the computed oxidation potentials for 1 with no acid. Moving to the right in the diagram shows the successive additions of acetic acid and the calculated equilibria for association with 1. The middle column shows the oxidation potentials for a singly-protonated species with acetate association. Experimentally, the first oxidation potential shifts 0.23 V from 1 to the first protonated species (peak a to peak b, Fig. 2), and computationally the shift is 0.2 V. In general, it appears that the computations underestimate the oxidation potential shifts and strengths of protonation/acetate stabilization, but the trends are consistent with experiment. With the addition of two equivalents of acetic acid, access is gained to the double-protonated species in the far-right column, and the first oxidation potential of this species is again shifted positive. The computations indicate peak d with the addition of two equivalents of acid is likely the second oxidation potential of both the single protonated species $[Mo_2(hpp)_3(Hhpp)(OAc)]^+$ and the double protonated species $[Mo_2(hpp)_2(Hhpp)_2(OAc)_2]^+$. Both oxidations lead to computationally stable dications and chemical reversibility as indicated experimentally with the observation on the return CV scan of reductions corresponding to the species in regions c, b, and the starting complex. With the addition of excess acid peak d becomes electrochemically irreversible as pointed out previously.

Scheme 3. DFT-calculated equilibria (to the right) and oxidation potentials (going down, vs. Fc/Fc⁺) for the addition of acetic acid to 1 in THF.

3.5 Association of trifluoroacetic acid with 1

The addition of 1 equivalent of TFA to a solution of 1 yielded peak **e** in addition to peaks **a** and **a'** (Fig. 5). This shift of peak **e** from peak **a** is more positive than the shift of peak **b** observed with acetic acid, consistent with the stronger acid strength of TFA and the weaker donor trifluoroacetate ion. An overlay illustrating the shifts from both acids is presented in Fig. 5. Note that if the interaction were a simple protonation without concomitant stabilization by the conjugate base, peaks **b** and **e** would occur at the same potential, being the same protonated species. The association of the less electron rich trifluoroacetate group with the protonated complex is the reason that the oxidation becomes more difficult.

Scheme 4 shows the computed equilibria and the oxidation potentials of the associated TFA species in an analysis similar to Scheme 3. In the presence of TFA the equilibrium favors association to {Mo₂}(H)(TFA), which is

calculated to be oxidized 0.12 V positive of the corresponding oxidation with AcOH. The experimental shift between these peaks is 0.16 V.

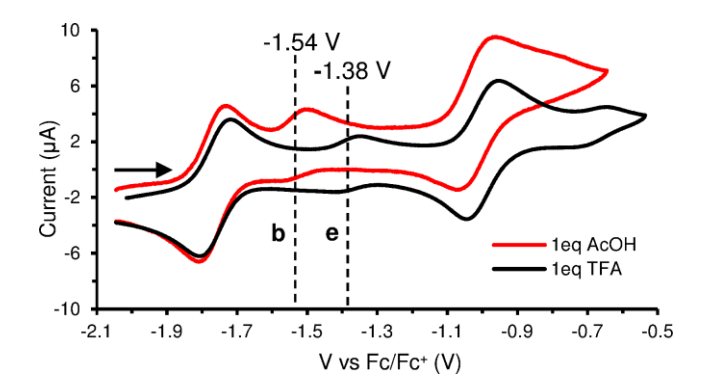


Fig. 5. Effect of trifluoroacetic acid on 2 mM 1 vs acetic acid (See Fig. 1 for conditions).

Scheme 4. DFT-calculated equilibria (to the right) and oxidation potentials (going down, vs Fc/Fc⁺) for the association of trifluoroacetic acid (TFA) and oxidations of 1 in THF

A comparison of the pK's in Schemes 3 and 4 shows that with moving to stronger acid the association is more favored. The equilibrium of $\{Mo_2\}$ to $\{Mo_2\}(H)(OAc)$ (top left reaction of Scheme 3) has a pK of -5, which favors association. That same equilibrium with TFA in Scheme 4 is 6 pK units more favorable (pK = -11). This trend continues onward towards the associated dication. Two equivalents of TFA drive the concentrations further to the right in the diagram such that peak \mathbf{e} weakens and additional oxidations are observed at more positive potentials (see SI).

Conclusions

The conclusions of this work are illustrated by the electrostatic potential map shown in Fig. 6. Areas of high electron density potential are shown in red and areas of positive potential are shown in blue. High electron density is found throughout the guanidinate core and into the δ -lobes of the metal–metal bond. These sites can be thought of as nucleophilic. Protons and hydrogen bonding are drawn to these nucleophilic sites. In contrast, the M–M axial sites are electrophilic, attracting electron pairs and anions. Hence these complexes are two-faced bifunctional, with a nucleophilic face in the guanidinate cores and an electrophilic face at the M–M axial sites. The HOMO and LUMO orbitals illustrate the elements of the frustrated Lewis pair (FLP). The HOMO contains the Lewis base sites and the LUMO represents the Lewis acid sites. These sites are constrained from each other by the rigidity of the structure rather than by steric repulsions of other FLPs. These two functional sites conspire together to protonate the complex. The most nucleophilic site is the nitrogen bound to the metals, which is the lowest energy site for hydrogen bonding and protonation. This interaction alone is not enough to deprotonate the acetic acid and protonate the complex. Protonation is thermodynamically favored once acetate association with the axial site is achieved. The path to this structure from the hydrogen bonding structure is facile. This is a novel example of synergism in chemical bonding; protonation is promoted by concomitant acetate association, and acetate association to the vacant axial site is promoted by protonation.

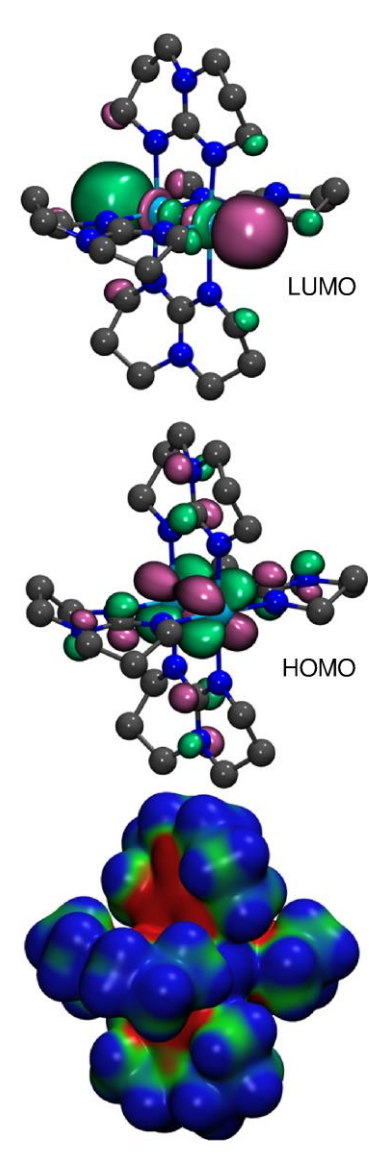


Fig. 6. The frontier orbitals of $Mo_2(hpp)_4$; An electrostatic potential map (bottom) shows nucleophilic sites (red) and electrophilic axial site (blue).

Acknowledgments

We gratefully acknowledge support from the National Science Foundation, Grant No. 1565207. All authors contributed to the writing of the manuscript.

Appendix A. Supplementary data

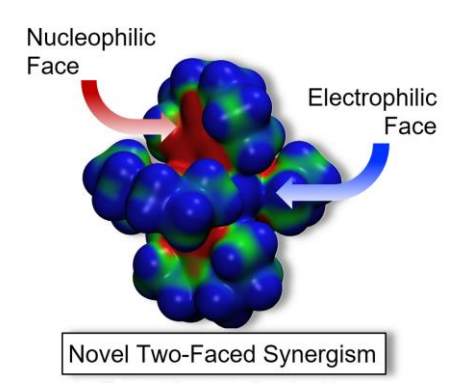
Scan rate studies of the first oxidation of Mo₂(TEhpp)₄ 1, CVs of 1 with one and two equivalents of trifluoroacetic acid, images of the protonated structures of 1 and the starting geometries for the transits for acetic acid approach to the complex, along with full DFT optimized geometry coordinates and transit coordinates in files for convenient visualization and animation, can be found in the supplementary data in the online version.

References

- [1] F.A. Cotton, J.C. Durivage, N.E. Gruhn, D.L. Lichtenberger, C.A. Murillo, D. Van Laura O., C.C. Wilkinson, Photoelectron Spectroscopy and DFT Calculations of Easily Ionized Quadruply Bonded Mo24+ Compounds and Their Bicyclic Guanidinate Precursors, J. Phys. Chem. B. 110 (2006) 19793–19798. doi:10.1021/jp061820m.
- [2] G.M. Chiarella, F.A. Cotton, J.C. Durivage, D.L. Lichtenberger, C.A. Murillo, Solubilizing the most easily ionized molecules and generating powerful reducing agents, J. Am. Chem. Soc. 135 (2013) 17889–17896.

- doi:10.1021/ja408291k.
- [3] F.A. Cotton, N.E. Gruhn, J. Gu, P. Huang, D.L. Lichtenberger, C.A. Murillo, L.O. Van Dorn, C.C. Wilkinson, D. Van Laura O., C.C. Wilkinson, Closed-Shell Molecules That Ionize More Readily Than Cesium, Sci. (Washington, DC, United States). 298 (2002) 1971–1975. doi:10.1126/science.1078721.
- [4] F.A. Cotton, C.A. Murillo, X. Wang, C.C. Wilkinson, Increasing the solubility of strong reducing agents containing Mo24+ units and alkyl-substituted guanidinate ligands, Dalton Trans. (2007) 3943–3951. doi:10.1039/b707201e.
- [5] N.G. Connelly, W.E. Geiger, Chemical Redox Agents for Organometallic Chemistry, Chem. Rev. 96 (1996) 877–910. doi:10.1021/cr940053x [doi].
- [6] J.A. Murphy, Discovery and Development of Organic Super-Electron-Donors, J. Org. Chem. 79 (2014) 3731–3746. doi:10.1021/j0500071u.
- [7] F.A. Cotton, L.M. Daniels, C.A. Murillo, D.J. Timmons, C.C. Wilkinson, The Extraordinary Ability of Guanidinate Derivatives to Stabilize Higher Oxidation Numbers in Dimetal Units by Modification of Redox Potentials: Structures of Mo25+ and Mo26+ Compounds, J. Am. Chem. Soc. 124 (2002) 9249–9256. doi:10.1021/jao266464 [doi].
- [8] F.A. Cotton, J.P. Donahue, N.E. Gruhn, D.L. Lichtenberger, C.A. Murillo, D.J. Timmons, L.O. Van Dorn, D. VillagrÃ;n, X. Wang, D. Van Laura O., D. Villagran, X. Wang, Facilitating Access to the Most Easily Ionized Molecule: an Improved Synthesis of the Key Intermediate, W2(hpp)4Cl2, and Related Compounds, Inorg. Chem. 45 (2006) 201–213. doi:10.1021/ic0515709.
- [9] M. Wang, L. Chen, L. Sun, Recent progress in electrochemical hydrogen production with earth-abundant metal complexes as catalysts, Energy Environ. Sci. 5 (2012) 6763–6778. doi:10.1039/c2ee03309g.
- [10] G.M. Chiarella, F.A. Cotton, S.A. Ibragimov, C.A. Murillo, C.C. Wilkinson, M.D. Young, Syntheses of very soluble alkylated bicyclic guanidinate ligands and structural characterization of a dipalladium paddlewheel, Polyhedron. 58 (2013) 7–12. doi:10.1016/j.poly.2012.06.002.
- [11] S. Usachev, A. Gridnev, Convenient preparation of bicyclic guanidines, Synth. Commun. 41 (2011) 3683–3688. doi:10.1080/00397911.2010.519848.
- [12] G. te Velde, F.M. Bickelhaupt, E.J. Baerends, C. Fonseca Guerra, S.J.A. van Gisbergen, J.G. Snijders, T. Ziegler, Chemistry with ADF, J. Comput. Chem. 22 (n.d.) 931–967. doi:10.1002/jcc.1056.
- [13] C.F. Guerra, J.G. Snijders, G. Te Velde, E.J. Baerends, Towards an Order-N DFT Method., Sect. Title Gen. Phys. Chem. 99 (1998) 391–403.
- [14] ADF2017.107, SCM, Theoretical Chemistry, Vrije Universiteit, Amsterdam, The Netherlands., (Http://Www.Scm.Com). (n.d.). http://www.scm.com.
- [15] E. van Lenthe, A. Ehlers, E.-J. Baerends, Geometry optimizations in the zero order regular approximation for relativistic effects, J. Chem. Phys. 110 (1999) 8943–8953. http://link.aip.org/link/?JCP/110/8943/1.
- [16] E. van Lenthe, E.J. Baerends, J.G. Snijders, Relativistic Total Energy Using Regular Approximations., J. Chem. Phys. 101 (1994) 9783–9792.
- [17] J.P. Perdew, K. Burke, M. Ernzerhof, Generalized Gradient Approximation Made Simple, Phys. Rev. Lett. 77 (1996) 3865–3868. http://link.aps.org.ezproxy1.library.arizona.edu/doi/10.1103/PhysRevLett.77.3865.
- [18] S. Grimme, S. Ehrlich, L. Goerigk, Effect of the damping function in dispersion corrected density functional theory, J. Comput. Chem. 32 (2011) 1456–1465. doi:10.1002/jcc.21759.
- [19] C.C. Pye, T. Ziegler, An implementation of the conductor-like screening model of solvation within the Amsterdam density functional package, Sect. Title Phys. Org. Chem. 101 (1999) 396–408.
- [20] A. Klamt, G. Schueuermann, COSMO: a new approach to dielectric screening in solvents with explicit expressions for the screening energy and its gradient, Sect. Title Gen. Phys. Chem. (1993) 799–805.
- [21] B. Delley, The conductor-like screening model for polymers and surfaces, Mol. Simul. 32 (2006) 117–123. doi:10.1080/08927020600589684.
- [22] N.L. Allinger, X. Zhou, J. Bergsma, Molecular mechanics parameters, J. Mol. Struct. THEOCHEM. 312 (1994) 69–83. doi:10.1016/S0166-1280(09)80008-0.
- [23] K. Andreas, The COSMO and COSMO-RS solvation models, Wiley Interdiscip. Rev. Comput. Mol. Sci. 1 (2011) 699–709. doi:10.1002/wcms.56.
- [24] S.S. Batsanov, Van der Waals Radii of Elements, Inorg. Mater. 37 (2001) 871-885. doi:10.1023/A:1011625728803.

- [25] F.A. Cotton, D.J. Timmons, New Multiply-Bonded Dimetal Compounds Containing Bridging 1,3,4,6,7,8-hexahydro-2H-pyrimido[1,2-a]Pyrimidinato Groups—I. The V24+, Cr24+ and Mo24+ Compounds and Some Salts of the Protonated Ligand, Polyhedron. 17 (1998) 179–184. http://www.sciencedirect.com/science/article/B6TH8-3SH46W5-W/2/4efi620e96516adfbo8561318634a655.
- [26] J.I. de la Cruz Cruz, P. Juarez-Saavedra, B. Paz-Michel, M. Leyva-Ramirez, A. Rajapakshe, A.K. Vannucci, D.L. Lichtenberger, M. Paz-Sandoval, Phosphine-Substituted (η -5-Pentadienyl) Manganese Carbonyl Complexes: Geometric Structures, Electronic Structures, and Energetic Properties of the Associative Substitution Mechanism, Including Isolation of the Slipped η -3-Pentadienyl Associative Intermedi, Organometallics. 33 (2014) 278. doi:10.1021/om401017t.
- [27] W. Humphrey, A. Dalke, K. Schulten, VMD Visual Molecular Dynamics, J. Molec. Graph. 14 (1996) 33–38.
- [28] F.A. Cotton, W. Wang, Preparation and Structure of Ditungsten Tetrabenzoate Bis(tetrahydrofuranate), Inorg. Chem. 21 (1982) 3859–3860. doi:10.1021/ico0140a058.
- [29] F.A. Cotton, P. Huang, C.A. Murillo, D.J. Timmons, A complete series of W2(hpp)4Cln (n = 0, 1, 2) compounds, Inorg. Chem. Commun. 5 (2002) 501–504. doi:10.1016/S1387-7003(02)00449-5.
- [30] R. Clerac, F.A. Cotton, L.M. Daniels, J.P. Donahue, C.A. Murillo, D.J. Timmons, Completion of the Series of M2(hpp)4Cl2 Compounds from W to Pt: The W, Os, and Pt Compounds, Inorg. Chem. 39 (2000) 2581–2584. doi:10.1021/ic991370v.
- [31] A.A. Oliferenko, P. V Oliferenko, J.G. Huddleston, R.D. Rogers, V.A. Palyulin, N.S. Zefirov, A.R. Katritzky, Theoretical Scales of Hydrogen Bond Acidity and Basicity for Application in QSAR/QSPR Studies and Drug Design. Partitioning of Aliphatic Compounds, J. Chem. Inf. Comput. Sci. 44 (2004) 1042–1055. doi:10.1021/ci0342932.
- [32] D.D. Beattie, A.C. Grunwald, T. Perse, L.L. Schafer, J.A. Love, Understanding Ni(II) Mediated C(sp3)-H Activation: Tertiary Ureas as Model Substrates, J. Am. Chem. Soc. 140 (2018) jacs.8bo7708. doi:10.1021/jacs.8b07708.
- [33] D. Lapointe, K. Fagnou, Overview of the Mechanistic Work on the Concerted Metallation–Deprotonation Pathway, Chem. Lett. 39 (2010) 1118–1126. doi:10.1246/cl.2010.1118.
- [34] F.A. Cotton, C.A. Murillo, R.A. Walton, Multiple Bonds Between Metal Atoms, Third Edition., Springer Science and Business Media, Inc., USA., 2005.
- [35] H. Chen, F.A. Cotton, Carboxylate exchange among dimolybdenum tetracarboxylates: The trifluoroacetate/formate system, 14 (1995) 2221–2224.
- [36] J. Lam, K.M. Szkop, E. Mosaferi, D.W. Stephan, FLP catalysis: main group hydrogenations of organic unsaturated substrates, Chem. Soc. Rev. (2018). doi:10.1039/C8CS00277K.



Electrochemical and computational studies of $Mo_2(TEhpp)_4$, a dimetal paddlewheel complex, show novel two-faced bifunctional synergism. Protonation of the nucleophilic face requires concomitant association of the conjugate base to the electrophilic face.

Scheme 1. The reactivity of 1 and 3 towards dechlorination of C–Cl bonds of dichloromethane and o-dichlorobenzene, respectively.

Scheme 2. Cyclization of **5** to form the ligand HTEhpp **6**.

- **Fig. 1.** Cyclic voltammogram of 1.1 mM 1 in 0.3 M nBu₄NPF₆ THF with $E_{1/2}$ values of -1.77 V for $[Mo_2]^{4+/5+}$ and -1.00 V for $[Mo_2]^{5+/6+}$ on a glassy carbon electrode (A = 0.071 cm²) at 100 mV s⁻¹ scan rate.
- **Fig. 2.** Cyclic voltammograms of 1 interacting with increasing concentrations of acetic acid. Black trace shows both redox events of 1 with no acid. The following traces show new quasi-reversible peaks indicating association of the acid to 1: red trace, 1 eq. acid; blue trace, 2 eq. acid; grey trace, 4 eq. acid. (See Fig. 1 for conditions)
- **Fig. 3.** Simplified bond line structure (top) and converged geometry (bottom) of the synergistic interaction where protonation at the nucleophilic position N_b on the bicyclic guanidinate is interdependently promoted by acetate bonding to the electrophilic Mo–Mo axial site with one oxygen, and the N_b -H group is H–bonding with the other oxygen atom of the acetate. The green lines show the primary electrostatic interactions, and the other hydrogen atoms of the hpp ligands are omitted for clarity.
- **Fig. 4.** Energy profile for association of acetic acid with $Mo_2(hpp)_4$. Path **a** is an approach of acetic acid toward the vacant axial site of the metal-metal bond. Path **b** is an approach of acetic acid perpendicular to the metal-metal bond and pointed at H-bond formation with an N_b atom of hpp. Region **c** is the synergistic stabilization obtained with acetate simultaneously oxygen-coordinating at the axial site and protonating the N_b site.

Scheme 3. DFT-calculated equilibria (to the right) and oxidation potentials (going down, vs. Fc/Fc^+) for the addition of acetic acid to 1 in THF.

Fig. 5. Effect of trifluoroacetic acid on 2 mM 1 vs acetic acid (See Fig. 1 for conditions).

Scheme 4. DFT-calculated equilibria (to the right) and oxidation potentials (going down, vs Fc/Fc⁺) for the association of trifluoroacetic acid (TFA) and oxidations of 1 in THF

Fig. 6. The frontier orbitals of Mo₂(hpp)₄ 1;. An electrostatic potential map (bottom) shows nucleophilic sites (red) and electrophilic axial site (blue).